

A Universal Wet-Chemistry Route to Metal Filling of Boron Nitride Nanotubes

Thang Pham,^{†,‡,||} Aidin Fathalizadeh,^{†,||} Brian Shevitski,^{†,§} Sally Turner,^{†,§,||} Shaul Aloni,[§] and Alex Zettl^{*,†,‡,||}

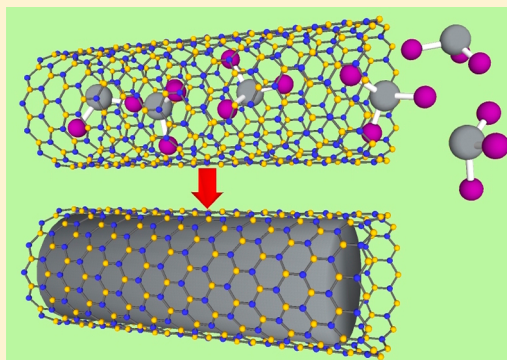
[†]Department of Physics, [‡]Department of Materials Science and Engineering, and [§]Department of Chemistry, University of California, Berkeley, California 94720, United States

^{||}Molecular Foundry and [¶]Materials Sciences Division, Lawrence Berkeley National Laboratory, Berkeley, California 94720, United States

^{*}Kavli Energy NanoSciences Institute at the University of California, Berkeley and the Lawrence Berkeley National Laboratory, Berkeley, California 94720, United States

S Supporting Information

ABSTRACT: We present a facile wet-chemistry method for efficient metal filling of the hollow inner cores of boron nitride nanotubes (BNNTs). The fillers conform to the cross-section of the tube cavity and extend in length from a few nm to hundreds of nm. The methodology is robust and is demonstrated for noble metals (Au, Pt, Pd, and Ag), transition metals (Co), and post-transition elements (In). Transmission electron microscopy and related electron spectroscopy confirm the composition and morphology of the filler nanoparticles. Up to 60% of BNNTs of a given preparation batch have some degree of metal encapsulation, and individual tubes can have up to 10% of their core volume filled during initial loading. The growth, movement, and fusing of metal nanoparticles within the BNNTs are also examined.



KEYWORDS: Boron nitride nanotubes, metal filling, wet-chemistry, metal nanowires

Over two decades ago, Broughton and Pederson¹ predicted that capillary forces are sufficient to drive a liquid into the inner cavity of a carbon nanotube (CNT). Since then, the filling of CNTs with metals, oxides, halides, and even biomolecules has been explored.^{2–7} The filler/CNT systems have been studied both theoretically and experimentally, demonstrating intriguing physical and chemical properties and potential applications in optoelectronics, nanothermometry, and catalysis.^{8–16} However, the conducting or semiconducting nature of a CNT, as well as its chemical reactivity, can induce undesirable interactions between the filler and the host, hindering the ability to investigate intrinsic properties (optical, electrical, and catalytic) of fillers,^{17–20} and limiting applications.

Boron nitride nanotubes (BNNTs) are wide-bandgap structural analogues to CNTs.^{21,22} They are electrically insulating, chemically inert, and have excellent thermal oxidation resistance and high mechanical strength.²³ This makes them attractive for studying the intrinsic properties of encapsulated materials or for constructing core–shell systems such as insulated nanocables. Despite these advantages, there have been only limited experiments on the filling of BNNTs.^{24–28} In the cases reported, filling is accomplished either *in situ* during the synthesis of the BNNTs²⁹ or *ex situ* (postsynthesis) using chemical vapor transport.²⁶ These methods severely restrict the filling material, for example,

materials used as catalysts for BNNT growth or those with a low vaporizing temperature. Additionally, low filling efficiencies make these methods far from ideal. A new method is needed, which can work for a variety of filler materials at mild conditions with higher filling yields and lower costs such as a solution-based approach. However, capillarity-induced filling of BNNTs using solution-based methods has not been reported; this is likely attributable to the greater difficulty in wetting the hexagonal BN surface compared to C.³⁰

In this report, we describe a successful wet-chemistry post-tube-synthesis route to the encapsulation of metallic nanostructures (including short nanocrystals, rods, and long wires) within BNNTs. As many as 60% of the BNNTs in the preparation batch have some degree of filling, with individual tubes having as much as 10% of their interior volume occupied by metal. We also explore the movement of metallic nanoparticles within the BNNT as well as the fragmenting and fusing of nanoparticles.

BNNTs used for the encapsulation in this study are first synthesized using the extended pressure inductively coupled (EPIC) plasma method.³¹ The BNNTs are largely double-

Received: September 23, 2015

Revised: December 8, 2015



ACS Publications

© XXXX American Chemical Society

A

DOI: 10.1021/acs.nanolett.5b03874
Nano Lett. XXXX, XXX, XXX–XXX

walled with high crystallinity and lengths up to several microns. The small inner diameters ($\sim 2\text{--}6$ nm) make them especially conducive to drawing in liquids via capillarity.³²

The BNNT ends, which are capped closed in as-synthesized material, are removed via acid treatment. The tubes are then placed in an ethanol bath containing metal salt precursors, wherein the salts enter the tube interior via capillary action. After drying, a thermal treatment reduces the metal salts yielding dense metal nanoparticles within the core of the BNNTs. The experiments here described are for a single-shot process (where only one filling step is performed), but the process can be repeated to enhance the overall filling factor of the tubes.

The metal-filled BNNTs are sonicated in isopropyl alcohol and drop cast onto lacey carbon grids for characterization by high-resolution transmission electron microscopy (HRTEM) and scanning transmission electron microscopy (STEM) (JEOL JEM 2010 operating at 80 kV and FEI Titan working at 80 and 120 kV). The composition of the product is evaluated with subnanometer resolution by a combination of energy dispersive X-ray (EDS) and electron energy loss (EELS) spectroscopies.

Figure 1, panel a shows a TEM image of a double-wall BNNT with etched open tip end before filling. Strong mineral

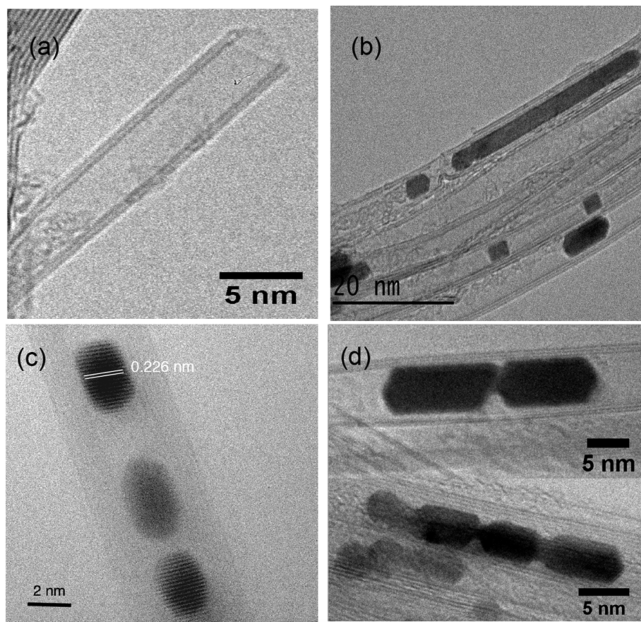


Figure 1. HRTEM images of (a) a double-wall BNNT with opened tip end after nitric acid treatment; (b) encapsulated Pt nanostructures within BNNTs; (c) Pt nanoparticles with lattice fringes corresponding to (111) planes; (d) nanosausage formed by sintering of Pt nanoparticles.

acids such as nitric acid have been used to selectively attack and remove the nanotube caps, which are sites of high chemical reactivity due to the incorporation of nonsix-membered rings.^{6,7,33} **Figure 1**, panel b is a representative TEM image of encapsulated Pt nanoparticles and nanorods within the BNNT cavity (denoted as Pt@BNNTs) prepared from H_2PtCl_6 . The metal nanostructure lengths range from 5–50 nm with a width normally defined by the inner diameter of the BNNTs (sub 10 nm as reported). **Figure 1**, panel c shows a zoomed-in image of an encapsulated Pt nanoparticle. The distance between lattice

fringes of the particles is 0.226 nm, which corresponds to the (111) lattice spacing of FCC Pt. The filling metals almost always conform to the inner cross-sectional area of the BNNTs, forming a leak-tight plug. As we demonstrate below, however, under the right circumstances, the plugs can be physically translated along the axis of the BNNT.

Other interesting structures are observed for metals formed within the BNNTs. **Figure 1**, panel d shows an example of sausage-shaped Pt rods with multiple neckings, conceivably the result of simultaneous growth of closely spaced Pt particles/rods during the reduction from proximate solutions. Another possibility for their formation is transport and subsequent end-to-end partial fusing of formerly separated particles, as suggested by Fan et al.^{34–37} The intriguing shapes of these marginally-coupled, segmented sausages and their relationship to plasmonic and catalytic properties are subjects for further investigation.

Similar results are obtained for other metal–salt precursors. For example, **Figure 2**, panels a and b show HRTEM images of

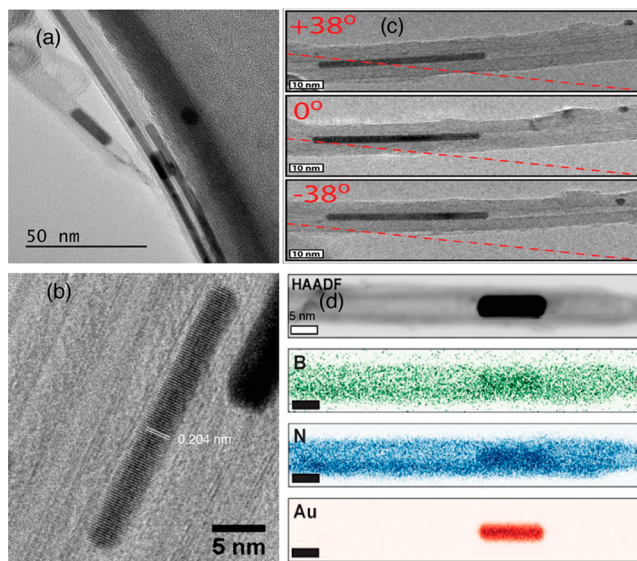


Figure 2. (a) TEM image of Au@BNNTs. Gold structures tend to form long nanorods instead of separated nanoparticles. (b) HRTEM of a single-crystallite Au nanorod with clear lattice fringes corresponding to (002) planes. (c) Series of TEM images of a sample tilted about the dashed red line confirming encapsulation of Au rod inside BNNT cavity. (d) STEM high-angle annular dark field image (contrast inverted for easier viewing) and EDS maps show chemical composition of filling material.

Au@BNNTs prepared from AuCl_3 . Gold nanostructures tend to form long nanorods with curved caps (as opposed to nanoparticles with distinct facets). As in the case of Pt@BNNT, the Au nanorods conform perfectly to the innermost walls of nanotubes. Au nanorod lengths range from 50–350 nm, with diameters 2–6 nm, the BNNT inner diameter range. Lattice fringes in the Au nanorod of **Figure 2**, panel b are spaced at 0.204 nm, corresponding to the (002) interplanar spacing of Au. The nanotube confinement creates very high aspect ratio Au nanorods without the need for any surface stabilizing ligands as prepared by other solution methods.^{38,39} These pure, nanoscaled, Au rods encapsulated by electronically and chemically inert BNNT are ideal subjects for studying nanoplasmonics.

To confirm the confinement and circular cross-section of formed metal nanostructures, TEM tilt-series are performed. Figure 2, panel c shows results for the Au@BNNT sample. The TEM sample stage is tilted 38° , forcing the nanotube to be rotated about the axis denoted by the dashed red line. While a small indexing particle clearly located on the outer surface of the tube (in the right corner of the images) sweeps out a circle and thus changes its projected position upon tilting, the core nanorod does not move with respect to the tube walls or change its diameter. This confirms that the metal nanorod is in the core of the BNNT. Additional evidence for tight metal nanorod confinement is provided by high-angle annular dark field (HAADF) STEM imaging, as shown in Figure 2, panel d.

Chemical composition of encapsulated materials is investigated using EDS and EELS. Representative results are shown in Figure 2, panel d for Au@BNNT. Elemental mapping using EDS highlights the distribution of elements (B, N, and Au) along the nanotube. As shown, elemental Au nanorods are confined inside the cavity of the BNNT. The EDS spectrum (Figure S2) confirms the purity of the metallic rod by showing only strong Au edges with only negligible traces of other precursor elements such as O or Cl. The apparent increase in the B and N signals corresponding to the Au nanoparticle is due to the increased Bremsstrahlung background in the spectral region of the B and N K shell edges.

Filling methods similar to those described above for Pt and Au are applied to prepare other metal-filled BNNTs including Pd@BNNT from PdCl_2 (Figure 3a), Ag@BNNT from AgNO_3

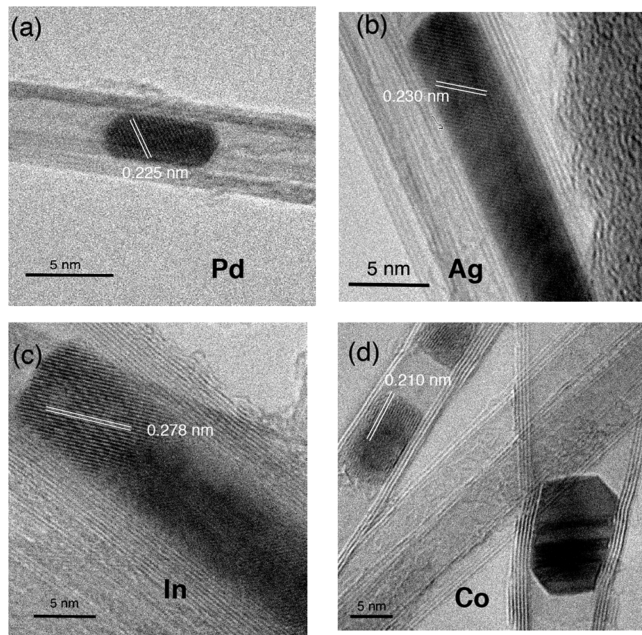


Figure 3. HRTEM images of other metal@BNNTs with denoted lattice spacings: (a) Pd, (b) Ag, (c) In, (d) Co.

(Figure 3b), In@BNNT from $\text{In}(\text{NO}_3)_3$ (Figure 3c), and Co@BNNT from $\text{Co}(\text{NO}_3)_2$ (Figure 3d). The identity of filling materials is confirmed by HRTEM and electron spectroscopy of the crystals. Figure 3, panel a clearly shows an encapsulated particle with sharp 120° facets and lattice fringes of 0.225 nm corresponding to the (111) interplanar spacings of FCC Pd. Much like Au, Ag filling forms almost exclusively nanorods as in Figure 3, panel b. The 30 nm long by 5 nm wide Ag rod

exhibits lattice fringes spaced at 0.230 nm, which matches the distance between (111) planes in Ag. The HRTEM image of In@BNNT in Figure 3, panel c shows a crystalline In particle forming a clear atomic interface with the innermost tubular shells. The spacing between lattice fringes is measured to be 0.278 nm, which corresponds to the (224) lattice spacing of tetragonal In. Similarly, Figure 3, panel d shows TEM images of encapsulated Co particles inside BNNTs. The particles conform nicely with the contour of BNNT innermost walls. The measured regular spacing of the observed planes of the lattice is 0.210 nm, which is consistent with the interplanar spacings of (100) HCP Co. These metal@BNNT systems are potential objects for study of nanoscaled plasmonic (Ag),⁴⁰ sensor (Pd),⁴¹ thermometer (In),⁴² and magnetism (Co).⁴³

Occasionally within the BNNTs we observe oxides of notably reactive metal particles, for example, In_2O_3 , as evidenced by the presence of O signals in EDS spectra. The oxidation occurs only at two ends of metal rods/particles (Figure S3). This indicates that a full conversion to an elemental metal has already taken place and that the oxidation of the nanowire ends is a result of interaction with ambient oxygen or less likely from products of the salt reduction confined in the BNNT following the H_2 reduction step.

The effect of thermal treatment temperature and time on metal crystal morphology and size was also investigated. Thermal treatments were conducted at 600, 700, 800, and 900 $^\circ\text{C}$ for 1, 2, and 4 h (under the same H_2 flow). Variations in the treatment temperature and time generally did not affect the metal structures and dimensions. This is likely because treatment temperatures are all well above the reduction temperature of the metal salts, preventing further evolution with increased treatment time beyond an already substantial base soak time. The metal structures and dimensions do, however, depend on the metals themselves, as discussed previously. For example, Pt tends to form particles, rods, and nanosausages, while Au tends to form very long nanowires.

In the series of TEM images of Figure 4, the inner cavity of BNNTs acts as a chamber within which electron beam irradiation induced phenomena can be observed. Particle nucleation can be seen at $t = 7\text{ s}$, indicated by solid yellow

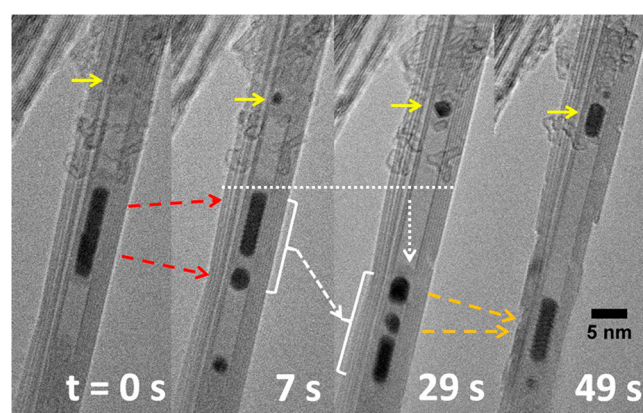


Figure 4. Nanotest tube environment revealing electron beam irradiation induced evolution of Au@BNNTs demonstrating nucleation and growth (solid yellow arrows near top of nanotube); splitting (dashed red arrows from $t = 0\text{ s}$ to 7 s); agglomeration (dashed orange arrows from $t = 29\text{ s}$ to 49 s); and splitting, agglomeration, and translation (white brackets connected by a dashed arrow from $t = 7\text{ s}$ to $t = 29\text{ s}$) of nanoscale Au particles.

arrows, with nanorod growth occurring near the top of the nanotube from $t = 0$ s to $t = 49$ s. Under electron beam irradiation, AuCl_3 molecules are reduced to Au (or Au ion) clusters.⁴⁴ These clusters will coalescence to form the nuclei of nanoparticle. Over time, more Au ion/atoms will be dissociated from the nearby AuCl_3 reservoir (amorphous-like substance at the top of images) and join the nuclei so that the particle grows bigger. Therefore, the gold indicated by solid yellow arrow nucleates and grows from AuCl_3 at the top of the tube, but not from the Au particles indicated by dashed red arrows. Near the top and the bottom of the images, there is AuCl_3 solution within the nanotubes, which under the electron beam will be reduced and form new Au particles. There might be some small Au clusters in the segment between the solid yellow arrow and dashed red arrows, but they cannot be resolved. The amorphous-like substance in the image is just amorphous carbon or residual solvent (isopropanol) since it disintegrates very quickly under the beam (from 7 to 29 s). Restricted to the low dimensional environment, nanoparticles are seen to split apart (dashed red arrows from $t = 0$ s to 7 s) and agglomerate (dashed orange arrows from $t = 29$ s to 49 s). From $t = 7$ s to 29 s, the nanoparticles and nanorods near the center translate down the tube axis, indicated by the dotted white arrow. In the process of shifting, the nanoparticles exhibit splitting and agglomeration as well (white brackets connected by a dashed arrow from $t = 7$ s to $t = 29$ s). This all occurs without any damage to the inner tube wall, indicating a low degree of friction between filler material and the inner cavity. As such, the BNNT serves as an inert nanoscaled chamber or test tube inside which chemical and mechanical interactions can be induced and studied.

We now turn to a more detailed examination of the solution-based filling process. We postulate that the combination of high crystallinity and small inner diameter BNNTs, and the use of low surface energy solvents, promotes solution filling by capillary force.³² In the case of CNTs, wetting and hence capillarity-driven filling in accordance with the Young–Laplace law occur for elements with a surface tension less than 100–200 mN/m.⁴ A nanoscale version of the Wilhelmy method with a BNNT based force sensor has measured the surface tension of a BNNT (27 mN/m) to be comparable to that of CNTs.⁴⁵ BNNTs with much larger diameters will have wetting properties approaching that of hBN sheets. The surface tensions of liquid metals explored in this study are significantly greater (560–1900 mN/m), suggesting the inability of the molten metals to physically flow into BNNTs without an applied pressure. A wet-chemistry approach overcomes these limits as metal–salt precursors dissolved in low surface tension solvents, such as ethanol (22 mN/m), can be introduced to the inside cavity of a BNNT by capillary force.

Furthermore, the small inner diameters (<10 nm) and highly crystalline nature of BNNTs synthesized by the EPIC plasma method enhance their ability to draw in liquids via capillarity.³² We find that BNNTs synthesized by other methods^{46,47} cannot easily be filled with metals using wet-chemistry methods, likely due to their large inner diameters (>50–80 nm) and often curvy or bamboo-like structures.⁴⁸ Size dependent filling behavior for different metals may also occur. For example, BN cavities filled by Ag are notably larger (~4–9 nm) than those containing Co fillings (~2–6 nm) (Figure S4). Similar size dependence has been observed for CNTs as well, where a threshold diameter is proposed for capillary filling of different materials based on a polarizability description of the wetting

conditions.³² Our measurements for diameter dependence of filled BNNTs is presented in Figure S4 for selected encapsulated metals.

Discrete nanorods or arrays of nanoparticles are formed throughout a tube cavity during thermal reduction as the contained metal–salt precursor's volume reduces to form the more dense metal fillings. Calculations (as shown in Supporting Information) of the reduction in volume from precursor to elemental metal indicate filling efficiencies obtained are close to their expected maximum value for some fillers. For instance, some individual BNNTs were filled up to 10 vol % with Au, compared to their calculated maximum filling factor of 15 vol %. The very high aspect ratio and bundling of BNNTs make the dependence of filling efficiency on nanotube length difficult to determine. Theoretical maximum filling yields utilizing wet-chemistry techniques have also been reported in the case of CNTs. During the solution-based filling procedure described above, solvent molecules will be encapsulated together with the metal salt precursors within BNNTs. Nonmetal filled regions will be left behind following thermal treatment due to the removal of these solvents and other resultant products formed during the thermal reduction of the metal–salt precursor.⁴⁹ The loading procedure may be repeated to enhance filling yields. Careful TEM investigation reveals that the metal nanoparticles form randomly along the interior length of the tubes, that is, there is no filling preference for the region near the ends of the tubes over the middle region of the tubes.

In conclusion, we demonstrate a simple but effective route to encapsulate nanoparticles and nanorods of various metals (Pt, Au, Pd, Ag, In, Co) within BNNTs by a postsynthesis wet-chemistry method for the first time. TEM, STEM, EDS, and EELS data confirm the successful filling of metals with crystalline structures and definite atomic boundaries within the nanotube shells. Previous methods have demonstrated some success in the filling of BNNTs, but only with a limited number of insertion materials, in particular those that serve as catalysts for the growth of BNNTs (Fe, Co)²⁵ or fillers with low vaporizing temperature (KCl).²⁶ Our simplified approach is versatile and applicable for a wide range of materials with various vaporizing temperatures, for example Pt, Au, Ag, Pd, In, and Co thus far. Moreover, previously reported methods have significantly lower filling yields (less than 30% versus 60% as in our report). They are also more expensive and time-consuming, for instance required the creation of ampoules and high temperature. Previously reported filling methods are inherently small batch processes, producing only a small (mg) amounts of final sample at a time. This makes such techniques largely unsuitable for large-scale application as would be required for using filled BNNTs for thermal management and composites. Our solution-based filling approach matches well with large-scale methods of producing BNNTs using plasma synthesis.^{31,50} For applications such as electromagnetic shielding composites, significant amounts of materials are required with high mechanical strength and thermal resistance, yet with some electrical conductance for absorbing electromagnetic radiation. Metal-filled BNNTs prepared by the current method meet these requirements. Moreover, the large quantity of metal filled BNNTs also finds promising applications in catalysts (Pt@BNNTs),⁵¹ hydrogen storage (Pd@BNNTs),⁵² plasmonic devices (Au@BNNTs),⁵³ thermal management (Ag@BNNTs),⁵⁴ and memory devices (Co@BNNTs).⁵⁵

It should be noted that previous methods for filling BNNTs also require high temperatures (600–1000 °C), which make

them incompatible for the filling of heat-sensitive chemicals and biomolecules. The present method is based on solution filling at room temperature, which is entirely suitable for biochemical molecules (water, proton, small ion, DNA).^{56,57} The filling of the inner pores of BNNTs with biochemical molecules could be the first step in enabling nanopore science based on BNNTs. BNNTs not only spatially confine the metal crystals, but also serve as an electrically and chemically inert shell to protect and enhance the stability of metal nanostructures. Hence, metals@BNNTs present new forms of nanoscaled metals with likely unusual optical, electric, catalytic, and magnetic properties.

■ ASSOCIATED CONTENT

Supporting Information

The Supporting Information is available free of charge on the ACS Publications website at DOI: [10.1021/acs.nanolett.5b03874](https://doi.org/10.1021/acs.nanolett.5b03874).

Synthesis of metals@BNNTs; HAADF STEM images and EDS/EELS spectra of Pt@BNNT, Au@BNNT, and In@BNNT samples; diameter dependence of BNNTs with different filling metals; calculation of theoretical maximum filling ([PDF](#))

■ AUTHOR INFORMATION

Corresponding Author

*E-mail: azettl@physics.berkeley.edu.

Author Contributions

T.P. and A.F. contributed equally to this work. The manuscript was written through contributions of all authors. All authors have given approval to the final version of the manuscript.

Notes

The authors declare no competing financial interest.

■ ACKNOWLEDGMENTS

This research was supported in part by the Director, Office of Basic Energy Sciences, Materials Sciences and Engineering Division, of the U.S. Department of Energy under Contract No. DE-AC02-05CH11231, within the sp-bonded Materials Program, which provided for the design, construction, and execution of the experiment; and by the Molecular Foundry at the Lawrence Berkeley National Laboratory, under Contract No. DE-AC02-05CH11231, which provided for STEM, EDS, and EELS characterization.

■ REFERENCES

- (1) Pederson, M. R.; Broughton, J. Q. *Phys. Rev. Lett.* **1992**, *69* (18), 2689–2692.
- (2) Ajayan, P. M.; Ebbesen, T. W.; Ichihashi, T.; Iijima, S.; Tanigaki, K.; Hiura, H. *Nature* **1993**, *362* (6420), 522–525.
- (3) Saito, Y.; Yoshikawa, T. *J. Cryst. Growth* **1993**, *134* (1–2), 154–156.
- (4) Dujardin, E.; Ebbesen, T. W.; Hiura, H.; Tanigaki, K. *Science* **1994**, *265* (5180), 1850–1852.
- (5) Tsang, S. C.; Chen, Y. K.; Harris, P. J. F.; Green, M. L. H. *Nature* **1994**, *372* (6502), 159–162.
- (6) Sloan, J.; Hammer, J.; Zwiefka-Sibley, M.; Green, M. L. H. *Chem. Commun.* **1998**, *3*, 347–348.
- (7) Monthioux, M. *Carbon* **2002**, *40* (10), 1809–1823.
- (8) Serp, P. *Appl. Catal., A* **2003**, *253* (2), 337–358.
- (9) Tasis, D.; Tagmatarchis, N.; Bianco, A.; Prato, M. *Chem. Rev.* **2006**, *106* (3), 1105–1136.
- (10) Monthioux, M.; Flahaut, E.; Cleuziou, J.-P. *J. Mater. Res.* **2006**, *21* (11), 2774–2793.
- (11) Eder, D. *Chem. Rev.* **2010**, *110* (3), 1348–1385.
- (12) Monteiro, A. O.; Cachim, P. B.; Costa, P. M. F. J. *Diamond Relat. Mater.* **2014**, *44*, 11–25.
- (13) Gao, Y.; Bando, Y. *Nature* **2002**, *415* (6872), 599.
- (14) Pan, X.; Fan, Z.; Chen, W.; Ding, Y.; Luo, H.; Bao, X. *Nat. Mater.* **2007**, *6* (7), 507–511.
- (15) Che, G.; Lakshmi, B. B.; Martin, C. R.; Fisher, E. R. *Langmuir* **1999**, *15* (3), 750–758.
- (16) Korneva, G.; Ye, H.; Gogotsi, Y.; Halverson, D.; Friedman, G.; Bradley, J.-C.; Kornev, K. G. *Nano Lett.* **2005**, *5* (5), 879–884.
- (17) Carter, R.; Sloan, J.; Kirkland, A. I.; Meyer, R. R.; Lindan, P. J. D.; Lin, G.; Green, M. L. H.; Vlandas, A.; Hutchison, J. L.; Harding, J. *Phys. Rev. Lett.* **2006**, *96* (21), 215501.
- (18) Grobert, N.; Hsu, W. K.; Zhu, Y. Q.; Hare, J. P.; Kroto, H. W.; Walton, D. R. M.; Terrones, M.; Terrones, H.; Redlich, P.; Rühle, M.; Escudero, R.; Morales, F. *Appl. Phys. Lett.* **1999**, *75* (21), 3363.
- (19) Corio, P.; Santos, A. P.; Santos, P. S.; Temperini, M. L. A.; Brar, V. W.; Pimenta, M. A.; Dresselhaus, M. S. *Chem. Phys. Lett.* **2004**, *383* (5–6), 475–480.
- (20) Kharlamova, M. V.; Yashina, L. V.; Lukashin, A. V. *J. Mater. Sci.* **2013**, *48* (24), 8412–8419.
- (21) Rubio, A.; Corkill, J.; Cohen, M. *Phys. Rev. B: Condens. Matter Mater. Phys.* **1994**, *49* (7), 5081–5084.
- (22) Chopra, N. G.; Luyken, R. J.; Cherrey, K.; Crespi, V. H.; Cohen, M. L.; Louie, S. G.; Zettl, A. *Science* **1995**, *269* (5226), 966–967.
- (23) Cohen, M. L.; Zettl, A. *Phys. Today* **2010**, *63* (11), 34–38.
- (24) Han, W.; Redlich, P.; Ernst, F.; Rühle, M. *Appl. Phys. Lett.* **1999**, *75* (13), 1875.
- (25) Golberg, D.; Xu, F.-F.; Bando, Y. *Appl. Phys. A: Mater. Sci. Process.* **2003**, *76* (4), 479–485.
- (26) Han, W.-Q.; Chang, C. W.; Zettl, A. *Nano Lett.* **2004**, *4* (7), 1355–1357.
- (27) Han, W.-Q.; Zettl, A. *Appl. Phys. Lett.* **2002**, *81* (26), 5051.
- (28) Mickelson, W.; Aloni, S.; Han, W.-Q.; Cumings, J.; Zettl, A. *Science* **2003**, *300* (5618), 467–469.
- (29) Tang, C.; Bando, Y.; Golberg, D.; Ding, X.; Qi, S. *J. Phys. Chem. B* **2003**, *107* (27), 6539–6543.
- (30) Bando, Y.; Ogawa, K.; Golberg, D. *Chem. Phys. Lett.* **2001**, *347* (4–6), 349–354.
- (31) Fathalizadeh, A.; Pham, T.; Mickelson, W.; Zettl, A. *Nano Lett.* **2014**, *14* (8), 4881–4886.
- (32) Ugarte, D.; Stöckli, T.; Bonard, J. M.; Châtelain, A.; de Heer, W. A. *Appl. Phys. A: Mater. Sci. Process.* **1998**, *67* (1), 101–105.
- (33) Datsyuk, V.; Kalyva, M.; Papagelis, K.; Parthenios, J.; Tasis, D.; Siokou, A.; Kallitsis, I.; Galiotis, C. *Carbon* **2008**, *46* (6), 833–840.
- (34) Wu, H.; Bai, F.; Sun, Z.; Haddad, R. E.; Boye, D. M.; Wang, Z.; Huang, J. Y.; Fan, H. *J. Am. Chem. Soc.* **2010**, *132* (37), 12826–12828.
- (35) Li, W.; Fan, H.; Li, J. *Nano Lett.* **2014**, *14* (9), 4951–4958.
- (36) Wu, H.; Bai, F.; Sun, Z.; Haddad, R. E.; Boye, D. M.; Wang, Z.; Fan, H. *Angew. Chem., Int. Ed.* **2010**, *49* (45), 8431–8434.
- (37) Li, B.; Wen, X.; Li, R.; Wang, Z.; Clem, P. G.; Fan, H. *Nat. Commun.* **2014**, *5*, 4179.
- (38) Jana, N. R.; Gearheart, L.; Murphy, C. J. *J. Phys. Chem. B* **2001**, *105* (19), 4065–4067.
- (39) Loubat, A.; Impérator-Clerc, M.; Pansu, B.; Meneau, F.; Raquet, B.; Viau, G.; Lacroix, L.-M. *Langmuir* **2014**, *30* (14), 4005–4012.
- (40) Ditlbacher, H.; Hohenau, A.; Wagner, D.; Kreibig, U.; Rogers, M.; Hofer, F.; Ausseneegg, F. R.; Krenn, J. R. *Phys. Rev. Lett.* **2005**, *95* (25), 257403.
- (41) Yang, F.; Taggart, D. K.; Penner, R. M. *Nano Lett.* **2009**, *9* (5), 2177–2182.
- (42) Gao, Y.; Bando, Y.; Golberg, D. *Appl. Phys. Lett.* **2002**, *81* (22), 4133.
- (43) Liu, Z.; Chang, P.-C.; Chang, C.-C.; Galaktionov, E.; Bergmann, G.; Lu, J. G. *Adv. Funct. Mater.* **2008**, *18* (10), 1573–1578.
- (44) Yuk, J. M.; Park, J.; Ercius, P.; Kim, K.; Hellebusch, D. J.; Crommie, M. F.; Lee, J. Y.; Zettl, A.; Alivisatos, A. P. *Science* **2012**, *336* (6077), 61–64.
- (45) Yum, K.; Yu, M.-F. *Nano Lett.* **2006**, *6* (2), 329–333.

- (46) Tang, C.; Bando, Y.; Sato, T.; Kurashima, K. *Chem. Commun.* **2002**, *12*, 1290–1291.
- (47) Huang, Y.; Lin, J.; Tang, C.; Bando, Y.; Zhi, C.; Zhai, T.; Dierre, B.; Sekiguchi, T.; Golberg, D. *Nanotechnology* **2011**, *22* (14), 145602.
- (48) Zhi, C.; Bando, Y.; Tang, C.; Golberg, D. *Mater. Sci. Eng., R* **2010**, *70* (3–6), 92–111.
- (49) Chen, Y. K.; Chu, A.; Cook, J.; Green, M. L. H.; Harris, P. J. F.; Heesom, R.; Humphries, M.; Sloan, J.; Tsang, S. C.; Turner, J. F. C. *J. Mater. Chem.* **1997**, *7* (3), 545–549.
- (50) Kim, K. S.; Kingston, C. T.; Hrdina, A.; Jakubinek, M. B.; Guan, J.; Plunkett, M.; Simard, B. *ACS Nano* **2014**, *8* (6), 6211–6220.
- (51) Wu, J. C. S.; Fan, Y.-C.; Lin, C.-A. *Ind. Eng. Chem. Res.* **2003**, *42* (14), 3225–3229.
- (52) Jhi, S.-H.; Kwon, Y.-K. *Phys. Rev. B: Condens. Matter Mater. Phys.* **2004**, *69*, 1.
- (53) Zhang, X.; Liu, H.; Tian, J.; Song, Y.; Wang, L. *Nano Lett.* **2008**, *8* (9), 2653–2658.
- (54) Hsu, P.-C.; Liu, X.; Liu, C.; Xie, X.; Lee, H. R.; Welch, A. J.; Zhao, T.; Cui, Y. *Nano Lett.* **2015**, *15* (1), 365–371.
- (55) Nagashima, K.; Yanagida, T.; Oka, K.; Taniguchi, M.; Kawai, T.; Kim, J.-S.; Park, B. H. *Nano Lett.* **2010**, *10* (4), 1359–1363.
- (56) Hilder, T. A.; Gordon, D.; Chung, S.-H. *Small* **2009**, *5* (19), 2183–2190.
- (57) Geng, J.; Kim, K.; Zhang, J.; Escalada, A.; Tunuguntla, R.; Comolli, L. R.; Allen, F. I.; Shnyrova, A. V.; Cho, K. R.; Munoz, D.; Wang, Y. M.; Grigoropoulos, C. P.; Ajo-Franklin, C. M.; Frolov, V. A.; Noy, A. *Nature* **2014**, *514* (7524), 612–615.